

Parity symmetry and energy spectrum of excitons in coupled self-assembled quantum dots

B. Szafran,* S. Bednarek, and J. Adamowski

Faculty of Physics and Nuclear Techniques, University of Mining and Metallurgy (AGH), Cracow, Poland

(Received 22 November 2000; published 5 September 2001)

A theoretical study is presented for excitons in coupled self-assembled InGaAs quantum dots. We have proposed a model of an isolated single quantum dot based on the assumption of the Gaussian distribution of indium concentration. The same distribution, with the parameters fixed for the single dot, has been applied to vertically stacked coupled quantum dots in order to study the exciton properties, which result from the interdot coupling. The exciton lowest-energy levels have been calculated with use of the many-element variational basis, which includes the two-particle correlation effects. We have discussed the symmetry with respect to the parity of the exciton wave functions in the coupled quantum dots. We have shown that—in a general case—these wave functions do not possess the definite one-particle parity. Only for very small interdot distance the ground-state wave function exhibits the approximate one-particle parity. The nature of splitting of the photoluminescence lines in the coupled quantum dots is discussed. The present theory applied to a description of photoluminescence spectra in coupled self-assembled InGaAs quantum dots leads to a very good agreement with the experimental data.

DOI: 10.1103/PhysRevB.64.125301

PACS number(s): 73.23.-b

I. INTRODUCTION

A three-dimensional confinement of charge carriers in semiconductor quantum dots (QD's) results in a space quantization of energy levels.¹ Electron systems confined in QD's are called artificial atoms,^{2,3} since they show atomiclike properties, e.g., their energy spectrum is discrete. Among various types of QD's, the self-assembled QD's are the subject of an extensive study^{4–28} because of their possible applications in semiconductor lasers. It is expected¹³ that the self-assembled QD's used as active regions in the semiconductor lasers will provide low-threshold currents, a high gain, and an improved thermal stability of the devices. The coupled QD's (Refs. 14–21) can be treated as artificial molecules. The coupling between the QD's should be useful in optical applications, because it leads to an appearance of additional spectral lines. The positions of these lines can be changed by choosing different interdot distances in a technological process.

The present study has been inspired by the recent measurements²¹ of exciton-related radiative transitions in vertically stacked InGaAs self-assembled QD's.²¹ The experimental results,²¹ obtained with use of the state-filling photoluminescence spectroscopy,²² show a strong dependence of the photoluminescence spectra on the distance between the dots. In the state-filling spectroscopy,²² the exciting light of large intensity is used to fill as many electron-hole states as possible; so, all the allowed radiative transitions can be detected. In recent measurements,^{9,10} carried out on a single self-assembled QD, the fine structure of the luminescence spectrum has been observed as a function of the excitation power, i.e., as a function of the number of the confined excitons. In the case of the coupled QD's, the experimental spectra²¹ have been taken from a sample containing a large number of QD's. Then, the fine structure is not observed, since the inhomogeneous broadening of the luminescence lines is larger than the fine-structure splitting⁹ and the energetic positions of the lines do not show any

visible dependence on the number of confined excitons. Therefore, at this level of the experimental resolution, a theory of a single exciton should be sufficient for the interpretation of these measurements.²¹

A theoretical description of the excitons in the single dots was elaborated for self-assembled InAs/GaAs QD's (Ref. 29) and for InP and CdSe nanocrystals³⁰ in the framework of the pseudopotential approach. In Ref. 31, the excitons in the coupled QD's were studied as candidates for a reliable preparation of entangled states in solid-state systems.

The present paper is devoted to theoretical study of parity symmetry and spectral properties of the exciton in isolated and coupled self-assembled quantum dots. The paper is organized as follows. In Sec. II, we formulate a theoretical model of the exciton in a single QD. In Sec. III, we generalize this approach to the case of the coupled QD's. In Sec. IV we present the results and discussion and in Sec. V we give the summary.

II. SINGLE QUANTUM DOT

In this section, we formulate and parametrize a model of a single QD, which will be used in the following sections for a description of exciton states in coupled QD's. Most of theoretical papers^{2,11,12,23–28} dealing with the QD's use the two-dimensional model of the QD. Such a model does not allow for a description of the coupling between vertically stacked QD's. In order to describe the coupling between the QD's aligned in the growth direction, we have proposed a three-dimensional model of a single, isolated $\text{In}_x\text{Ga}_{1-x}\text{As}$ QD. The present model is based on the recent understanding³² of the growing process of the self-assembled QD's. During the growing process, InAs deposited on the GaAs substrate first forms a thin wetting layer and next InAs island. This nanostructure is subsequently covered with GaAs. Due to the indium diffusion³² the self-assembled QD's are made of the $\text{In}_x\text{Ga}_{1-x}\text{As}$ alloy with a spatially varying indium concentration. In this paper, we propose a model that takes into

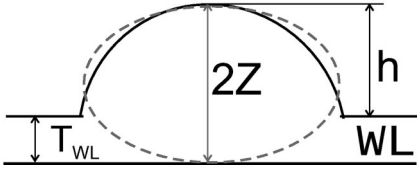


FIG. 1. Schematic of a single QD. Dashed line shows the contour of the indium-concentration Gaussian distribution function with range Z in the growth direction, h is the height of the QD and T_{WL} is the thickness of the wetting layer (WL).

account a spatial modulation of the indium concentration in the nanostructure. The present model is based on the assumption of the Gaussian distribution of indium concentration in the QD. Explicitly, we assume that indium concentration X in the single isolated QD is described by the Gaussian function of the cylindrical symmetry

$$X(\rho, z) = X_0 \exp(-\rho^2/R^2 - z^2/Z^2), \quad (1)$$

where $\rho^2 = x^2 + y^2$, X_0 is the indium concentration at the center of the dot, R is the dot "radius," and Z is the half of its "height." The real self-assembled QD's are not symmetric with respect to the inversion of the z axis (Fig. 1). Therefore, parameter $2Z$ can be treated as the effective height of the dot, which partially takes into account the presence of the wetting layer (Fig. 1). The $\text{In}_x\text{Ga}_{1-x}\text{As}$ island in the GaAs matrix is responsible for the potential confining the charge carriers in the quantum dot. The conduction-valence-band offset ratio for the InAs/GaAs interface was estimated to be 70/30.³³ Therefore, we assume the confinement potential to be parametrized as follows:

$$V_e(\rho, z) = -0.7\Delta E_g X(\rho, z) \quad (2)$$

for the electrons and

$$V_h(\rho, z) = -0.3\Delta E_g X(\rho, z) \quad (3)$$

for the holes, where $\Delta E_g = E_g^{\text{GaAs}} - E_g^{\text{InAs}}$, E_g^{GaAs} , and E_g^{InAs} are the GaAs and InAs energy gaps, respectively. In the present calculations, we take on $E_g^{\text{GaAs}} = 1.5196$ eV (Ref. 34) and $E_g^{\text{InAs}} = 0.4105$ eV.³⁵

Here, we briefly comment on the choice of the confinement potential [Eqs. (2) and (3)]. The application of the cylindrically symmetric Gaussian potential allows us to describe the three-dimensional confinement of the charge carriers in the QD's, and to take into account a finite depth of the confinement potential and an approximate parabolicity of the potential near the dot center. The properties of the one- and two-electron systems in the spherically symmetric, Gaussian confinement potential have been studied in detail in our recent paper.³⁶

Finally, in accordance with the assumed indium-concentration distribution [Eq. (1)], we introduce the following space dependence of the electron and hole effective masses:

$$m_{e,h}(\rho, z) = m_{e,h}^{\text{InAs}} X(\rho, z) + m_{e,h}^{\text{GaAs}} [1 - X(\rho, z)], \quad (4)$$

where $m_e^{\text{InAs}} = 0.023m_0$,³⁷ $m_e^{\text{GaAs}} = 0.0667m_0$,³⁸ $m_h^{\text{InAs}} = 0.41m_0$,³⁹ $m_h^{\text{GaAs}} = 0.5m_0$,⁴⁰ and m_0 is the electron rest mass.

Equations (2)–(4) express the effective confinement potentials for electrons and holes and the spatial modulation of their band masses by a single indium distribution function (1). The parameters of this function (X_0 , R , and Z) will be extracted from the experimental photoluminescent data for a single isolated QD. Such a procedure implicitly takes into account the strain effects⁷ and the indium concentration given by Eq. (1) has an effective meaning. The same parametrization, with values of parameters fixed for a single dot, will be applied to coupled double QD's. Therefore, the Gaussian distribution function [Eq. (1)] can be treated as an universal function, which allows us to include the most important effects for the real nanostructures.

In the case of the position-dependent effective masses,⁴¹ the Hamiltonian of the electron-hole pair confined in the single QD has the following form (in atomic units):

$$H = -\frac{1}{2} \nabla_e \frac{1}{m_e(\mathbf{r}_e)} \nabla_e + V_e(\rho_e, z_e) - \frac{1}{2} \nabla_h \frac{1}{m_h(\mathbf{r}_h)} \nabla_h + V_h(\rho_h, z_h) - \frac{1}{\epsilon r_{eh}}, \quad (5)$$

where \mathbf{r}_e and \mathbf{r}_h are the position vectors of the electron and hole, respectively, and $r_{eh} = |\mathbf{r}_e - \mathbf{r}_h|$. Since the dielectric properties of GaAs and InAs are similar, we have adopted the average value⁵ $\epsilon = 12.5$ of the static dielectric constant for the $\text{In}_x\text{Ga}_{1-x}\text{As}$ alloy for all values of X . Throughout the present paper, the conduction-band minimum of GaAs is the reference energy level for the electron and the GaAs valence-band maximum is the reference energy level for the hole [cf. Eqs. (2) and (3)].

Probability p of radiative transition from the exciton state described by the wave function $\Phi(\mathbf{r}_e, \mathbf{r}_h)$ is proportional to the integral⁴²

$$p \sim \left| \int d\mathbf{r}_e d\mathbf{r}_h \Phi(\mathbf{r}_e, \mathbf{r}_h) \delta(\mathbf{r}_e - \mathbf{r}_h) \right|^2. \quad (6)$$

In the present paper, we consider the optically active exciton states, i.e., the states, from which the radiative transitions (electron-hole recombination) are allowed. For these transitions the initial states correspond to zero total angular momentum, since otherwise integral (6) vanishes.

We note that Hamiltonian (5) commutes with the operator of the z component of the total angular momentum and the parity operator. Both these quantities are conserved in the framework of the present model. However, because of the presence of the Coulomb-interaction potential in Eq. (5), the one-particle operators of parity and z component of angular momentum do not commute with the Hamiltonian. Due to the small size of the self-assembled QD's the one-particle energies are considerably larger than to the Coulomb-interaction contribution. Moreover, the energy separations between the one-particle shells of different angular momenta are also large with respect to the Coulomb term. On the contrary, in the coupled QD's, the energy spacings between

the one-particle states of opposite parities can be arbitrarily small. Thus, it should be expected that the Coulomb interaction essentially perturbs the one-particle parity. In this paper, we concentrate our attention on the problem of parity, which arises for the coupled QD's. Therefore, we construct the exciton wave functions of zero total angular momentum, using the eigenstates of one-particle angular momentum, which is a reasonable approximation in the problem considered. We shall label the exciton states by the one-particle z -component angular momentum quantum number m and use the following dependence of the wave function $\Psi(\mathbf{r}_e, \mathbf{r}_h)$ on azimuthal angles φ_e and φ_h :

$$\chi_m(\varphi_e, \varphi_h) = \exp[im(\varphi_e - \varphi_h)]. \quad (7)$$

In the following, we consider the lowest-energy optically active exciton states with $m=0, 1, 2$, and 3 labeled by s, p, d , and f , respectively. In Eq. (7), the signs of the angular momentum quantum number for the electron and the hole are chosen to be opposite, i.e., z component of the total angular momentum for the exciton is zero. All the states considered are symmetric with respect to the in-plane inversion, i.e., the change of sign of x and y coordinates of both the particles. Therefore, the total parity of the exciton is entirely determined by the z parity.

The eigenvalue problem for the exciton confined in the single QD has been solved by variational means with the trial wave function of the form

$$\begin{aligned} \Phi_1(\mathbf{r}_e, \mathbf{r}_h) &= \rho_e^m \rho_h^m \chi_m(\varphi_e, \varphi_h) \\ &\times \sum_{jklm} c_{jklm} f_{jklm}(\rho_e, \rho_h, z_e, z_h, z_{eh}), \end{aligned} \quad (8)$$

which is expanded in the Gaussian basis

$$\begin{aligned} f_{jklm}(\rho_e, \rho_h, z_e, z_h, z_{eh}) &= \exp(-\alpha_j^e \rho_e^2 - \alpha^h \rho_h^2 - \beta_k^e z_e^2 \\ &\quad - \beta_l^h z_h^2 - \gamma^z z_{eh}^2), \end{aligned} \quad (9)$$

where $z_{eh} = z_e - z_h$. In Eq. (9), variational parameters α_j^e and α^h (β_k^e and β_l^h) describe the localization of the electron and the hole in the x - y plane (z direction), and γ^z accounts for the correlation of the relative motion in the z direction. Wave function Φ_1 partially includes the radial correlation between the electron and hole, since it cannot be separated into a product of ρ_e and ρ_h dependent functions. However, it neglects the angular correlation.

In order to check a quality of trial wave function (8) we have performed test calculations for the exciton ground-state energy E_0 using a more general variational wave function, which explicitly includes the in-plane electron-hole distance. For $m=0$ this wave function has the form

$$\begin{aligned} \Phi_0(\mathbf{r}_e, \mathbf{r}_h) &= \sum_{jklm} c_{jklm} \exp(-\alpha_j^e \rho_e^2 - \alpha_k^h \rho_h^2 - \beta_l^e z_e^2 - \beta_n^h z_h^2 \\ &\quad - \gamma_p^e \rho_{eh}^2 - \gamma^z z_{eh}^2), \end{aligned} \quad (10)$$

where $\rho_{eh}^2 = (x_e - x_h)^2 + (y_e - y_h)^2$ and variational parameters γ_p^e are responsible for the in-plane correlation. Putting

TABLE I. Convergence of ground-state energy estimates E_0 for an exciton confined in a single QD with increasing number of basis elements. In the first five columns, the upper limits of the corresponding sums in Eq. (10) are listed. According to Eq. (10), labels j, k, l, n , and p denote the different Gaussians dependent on ρ_e, ρ_h, z_e, z_h , and ρ_{eh} , respectively. N is the total number of basis elements used in the calculations. The numbers in the first row correspond to basis (8) used in the latter part of the present paper. Energy is expressed in meV.

j	k	l	n	p	N	E_0
2	2	3	2		24	-241.93
3	3	4	4		144	-242.22
3	3	4	4	1	144	-243.21
3	3	4	4	2	288	-243.59
3	3	4	4	3	432	-243.70

$\gamma_p^e = 0$ in Eq. (10) we obtain wave function (8) for $m=0$. The results of the test calculations reported in Table I show that the neglect of the angular correlation yields the ground-state energy estimate with the uncertainty less than 2 meV. For comparison the estimated widths of photoluminescence peaks²¹ amount to several meV. Therefore, basis (8) with the neglected angular correlation and smaller number of elements (cf. Table I) is sufficient for the present purposes. The results presented in this paper have been obtained with the use of basis (8), in which the sums run over $j, k, n=1, 2, l=1, \dots, 3$, and $p=0$ (cf. Table I). The energy eigenvalues E_m calculated for given angular momentum quantum number m are used to determine the energy of the radiative interband transition, which is defined as $h\nu_m = E_g^{\text{GaAs}} + E_m$.

The values of the parameters describing the indium-concentration distribution in Eq. (1) have been obtained from the adjustment of the calculated transition energies to the experimental data²¹ for the isolated QD's. For this purpose we have used the photoluminescence spectrum²¹ taken at the interdot distance of ~ 15 nm, for which the QD's can be treated as spatially separated and uncoupled. The values obtained are $X_0=0.66$, $Z=0.92$ nm, and $R=24.9$ nm. The comparison of the calculated and measured²¹ radiative-transition energies for the isolated quantum dot is presented in Table II. The further description of the vertical coupling

TABLE II. Calculated energy eigenvalues E_m of the optically active exciton states for the single QD, energy spacings ΔE between the consecutive energy levels, and calculated radiative-transition energies $h\nu_{calc}$. The measured transition energies $h\nu_{expt}$ are extracted from the photoluminescence-peak positions (Ref. 21) taken for the separated QD's ($a=15$ nm). The states involved in the transitions are quoted in the first column. Energy is expressed in meV.

	E_m	ΔE	$h\nu_{calc}$	$h\nu_{expt}$
s - s	-241.9		1277.7	1278.2
p - p	-197.2	44.8	1322.4	1322.2
d - d	-159.7	37.5	1359.9	1359.4
f - f	-125.9	33.8	1393.7	1394.4

TABLE III. Calculated lowest-energy levels of the electron, E_e , and hole, E_h , states in the single QD (the mutual Coulomb interaction omitted). The separations $\Delta E_{e,h}$ between the consecutive energy levels are also quoted. Energy is expressed in meV.

	E_e	ΔE_e	E_h	ΔE_h
s	-118.3		-101.4	
p	-89.0	28.3	-93.0	8.5
d	-64.1	25.9	-84.7	8.3
f	-40.7	23.4	-76.6	8.1

between the QD's requires an accurate modeling of the confinement in the growth direction. In this context, we have to emphasize that the value of Z we have obtained from our fit very well agrees with the experimental result.²¹ The height h of the dot was estimated by the transmission-electron spectroscopy²¹ to be smaller than 2 nm, whereas the wetting-layer thickness $T_{WL}=0.54$ nm (Ref. 21) (cf. Fig. 1, where $h=2Z-T_{WL}$). Table II shows that the differences between the calculated and measured radiative-transition energies do not exceed 0.5 meV, which is considerably less than the experimental uncertainty.

Table II shows that energy spacings ΔE between the subsequent energy levels decrease with the increasing energy of the interband transitions. According to our interpretation, three effects of comparable importance are responsible for this behavior. If the energy of the electron-hole pair state increases, the charge carriers become more weakly localized and in consequence (i) the effect of the nonparabolicity of the confinement potential becomes stronger,³⁶ (ii) the electron and hole effective masses become larger with the increasing distance from the dot center [cf. Eq. (4)], (iii) the Coulomb interaction between the confined charge carriers decreases. In Table III, we have listed the energy levels of the quantum-dot confined electron and hole calculated with the neglect of their mutual Coulomb interaction. The spacings between the hole energy levels are much smaller than those for the electron, which results from the larger effective mass of the hole. We also see that—contrary to the case of the parabolic confinement—the energy levels are not equally spaced. The effective nonparabolicity of the confining potential is considerably smaller for the hole, which results from the larger localization of the heavy hole near the dot center.

III. COUPLED QUANTUM DOTS

The parametrization obtained in Sec. II for the single QD enables us to discuss exciton states in coupled QD's. For this purpose we have extended the model formulated in Sec. II to the case of vertically stacked QD's. Accordingly, the indium-concentration distribution in the two coupled, vertically stacked QD's has been expressed as follows:

$$X(\rho, z) = X_0 \exp[-\rho^2/R^2 - (z-a/2)^2/Z^2] + X_0 \exp[-\rho^2/R^2 - (z+a/2)^2/Z^2], \quad (11)$$

where a is the distance between the centers of the QD's. We note that the model of the coupled QD's does not contain any

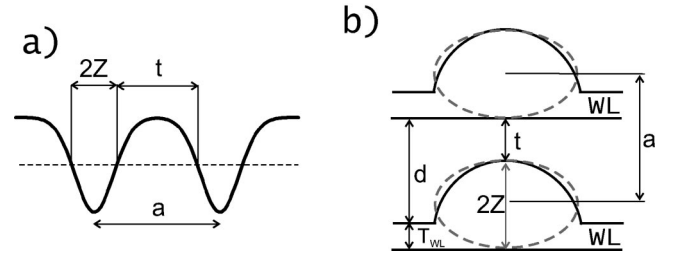


FIG. 2. Schematic of coupled QD's. The barrier and spacer thicknesses are denoted by t and d , respectively, a is the interdot-center distance. Plot (a) shows the profile of the confinement potential in the growth direction and plot (b) shows the geometry of the two coupled dots.

new fitting parameter. The shape of the potential confining the charge carriers in the coupled QD's, obtained from Eqs. (2) and (11), is schematically displayed in Fig. 2(a). Figure 2(b) shows the geometry of the coupled-dot nanostructure. In Eq. (11), the values of parameters X_0 , R , and Z are the same as for the single QD (Sec. II). In this section, we are using the same formulas for the confinement potentials, effective masses, and Hamiltonian as those given in Sec. II. In these formulas, we substitute concentration distribution function (1) by Eq. (11). For the exciton confined in the coupled quantum dots we propose the following trial wave function:

$$\begin{aligned} \Phi_2(\mathbf{r}_e, \mathbf{r}_h) &= \rho_e^m \rho_h^m \chi_m(\varphi_e, \varphi_h) \\ &\times \sum_{n_e=0}^1 \sum_{n_h=0}^1 \sum_{jklm} c_{jklm}^{n_e n_h} f_{jklm}[\rho_e, \rho_h, z_e \\ &+ (-1)^{n_e}(a/2), z_h + (-1)^{n_h}(a/2), z_{eh}], \quad (12) \end{aligned}$$

which is a generalization of the form given by Eq. (8). Wave function (12) allows for a description of the electron and hole states of both even and odd parity. Due to the presence of the Coulomb-interaction term in Hamiltonian (5), the exact wave functions are *not* eigenfunctions of the one-particle parity operators. Therefore, they do not possess a definite symmetry with respect to the change of sign of the z coordinate of one particle only. However, Hamiltonian (5) is invariant with respect to the simultaneous change of sign of both the coordinates z_e and z_h . Thus, the electron-hole wave functions possess a definite *total* parity. The symmetry with respect to the total parity applied to Eq. (6) yields the following selection rules: radiative transition is allowed (forbidden) for the initial state of even (odd) parity. Therefore, only the states of the even total parity are optically active.

The thickness of the barrier between the QD's is a more appropriate parameter for a description of the interdot coupling than the distance between the dot centers, since the self-assembled QD's do not possess well-defined centers. In the framework of the present model, thickness t of the interdot barrier is defined as follows: $t=a-2Z$ [cf. Fig. 2(a)], where a is the interdot-center distance. The experimental results²¹ have been given as functions of spacer thickness d . These two parameters are related by $t=d+T_{WL}-2Z$

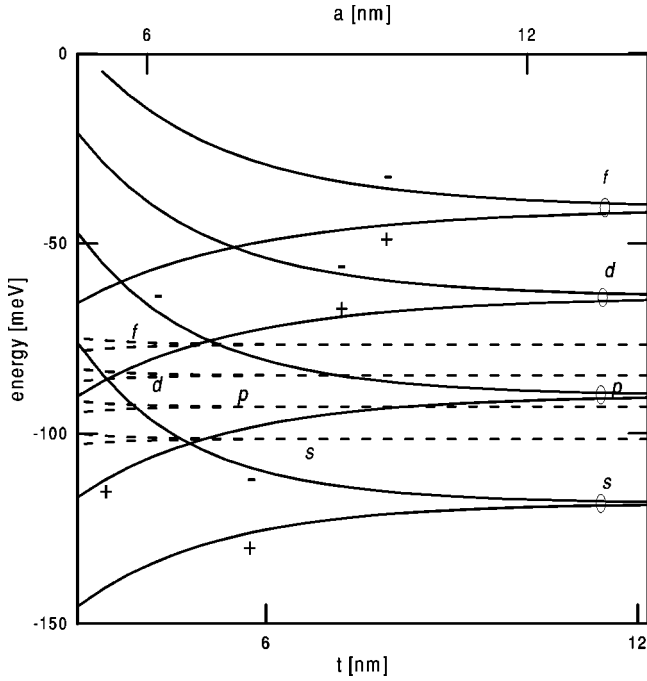


FIG. 3. Calculated one-particle energy levels of the electron (solid curves) and the hole (dashed curves) as functions of barrier thickness t (distance a between the centers of the dots). Signs $+$ and $-$ correspond to the states of even and odd z parity, respectively, and symbols s , p , d , and f denote the angular momentum quantum numbers $m=0, 1, 2$, and 3 , respectively.

[cf. Fig. 2(b)], which yields the following relation between the spacer thickness and the interdot-center distance: $d = a - T_{WL}$.

IV. RESULTS AND DISCUSSION

In Fig. 3, we have plotted the calculated energy levels of the electron and hole confined in the coupled QD's (with the electron-hole Coulomb interaction omitted) as functions of the barrier thickness (interdot-center distance). For large interdot distances the energy levels are twofold degenerate. When the distance between the dots decreases, the degeneracy with respect to the parity is lifted. The energies of even- (odd-) parity states decrease (increase) with the decreasing interdot separation. The resulting splitting of the energy levels is much larger for the electron than for the hole and only weakly depends on the angular-momentum quantum number.

Figure 4 presents the dependence of the eight lowest-energy levels for the s and p states of the exciton confined in the coupled QD's (with the Coulomb interaction included) on the barrier thickness. The solid curves correspond to the optically active states of even total parity and the dashed curves correspond to the states of odd total parity, from which the radiative transitions are forbidden. For large barrier thickness the lowest-energy s and p levels as well as the higher-energy levels are twofold degenerate. This degeneracy is lifted by the interdot coupling for small interdot separations. In the limit $t \rightarrow \infty$ the exciton ground-state energy becomes equal to the ground-state energy of the exciton

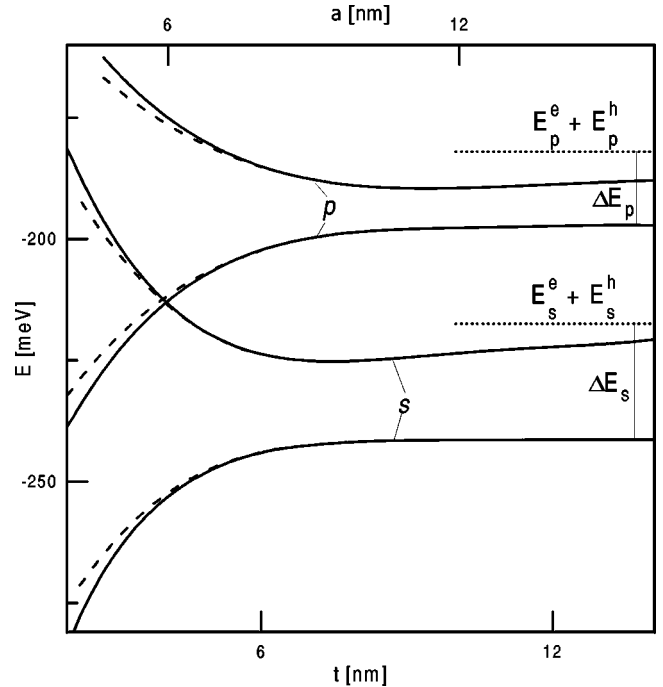


FIG. 4. Calculated energy of s and p states of the exciton confined in the coupled $\text{In}_x\text{GaAs}_{1-x}$ QD's as a function of barrier thickness t (interdot-center distance a). Solid (dashed) curves show the results for the even-parity optically active (odd-parity optically inactive) states. Dotted lines (labeled by $E_s^e + E_s^h$ and $E_p^e + E_p^h$) display the sums of the energies of the electron and the hole localized in the different infinitely separated QD's. ΔE_s and ΔE_p are the electron-hole Coulomb-interaction energies for s and p states, respectively.

confined in the single QD (cf. Table I). Similarly, the energy of lower p level becomes equal to the energy of p state of the exciton in the separated QD (cf. Table II). In the same limit, the higher-energy levels of both angular symmetries tend to the corresponding sums of the energies for the noninteracting electron and hole confined in the separated QD's (cf. Table II). These limit values marked by the dotted lines in Fig. 4 correspond to the dissociated exciton.

Figures 5, 6, and 7 display the contours of the probability amplitudes, i.e., the electron-hole wave functions $\Phi_2(\mathbf{r}_e = (0,0,z_e), \mathbf{r}_h = (0,0,z_h))$ for the four lowest-energy states of s symmetry. In these figures, the coordinates corresponding to the centers of the QD's are marked by the dashed straight lines and the white (dark gray) areas correspond to the lowest (highest) values of the wave functions [in plots (a) through (d), the shades of gray do not correspond to the same values of the wave function]. Figures 5, 6, and 7 show the asymmetry in the electron and hole probability distribution, which results from the stronger localization of the hole due to its larger mass.

Let us consider the case of large interdot distances (Fig. 5). In the two lowest-energy degenerate states [Figs. 5(a) and 5(b)], the values of Φ_2 differ only in signs, i.e., these states are characterized by the same probability density. The identical property holds true for the two degenerate excited states [cf. Figs. 5(c) and 5(d)]. The probability amplitudes for the

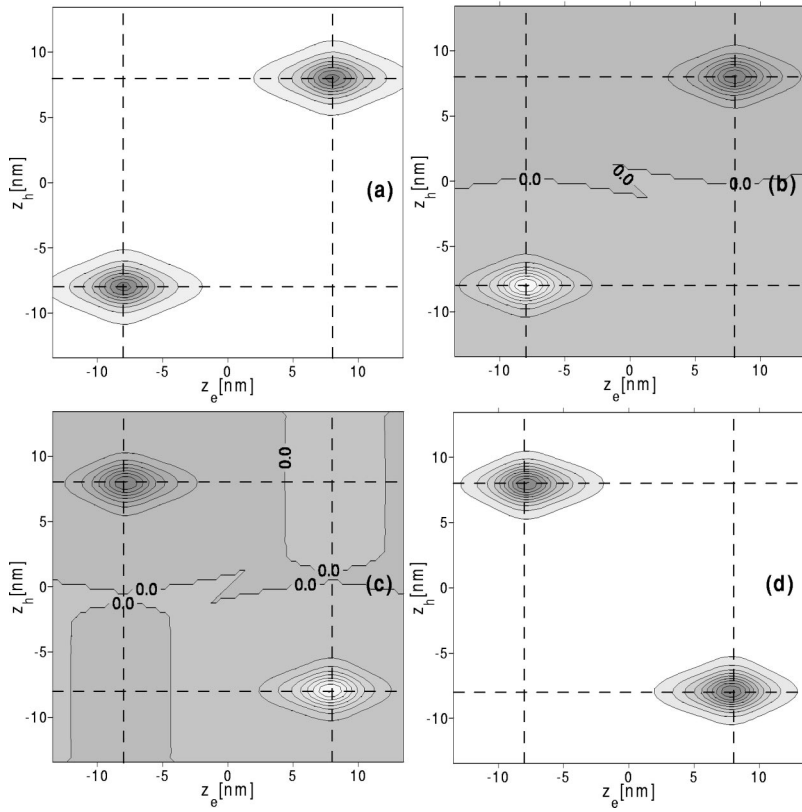


FIG. 5. Contours of s exciton wave functions $\Phi_2(\mathbf{r}_e=(0,0,z_e),\mathbf{r}_h=(0,0,z_h))$ for interdot-center distance $a=16$ nm, plotted along the z axis as functions of the electron z_e and hole z_h coordinates for (a) the ground state and the (b) first, (c) second, and (d) third excited state. White (dark gray) areas correspond to the lowest (highest) values of the wave functions. The shades of gray express the relative values of the wave functions, but are not the same in plots (a)–(d). In plots (a) and (d) [and also in 6(a) and 7(a)], the wave functions equal zero in the white areas, whereas in all the other plots the contours corresponding to the wave function equal to zero are denoted by 0.0. Dashed straight lines correspond to the coordinates of the dot centers.

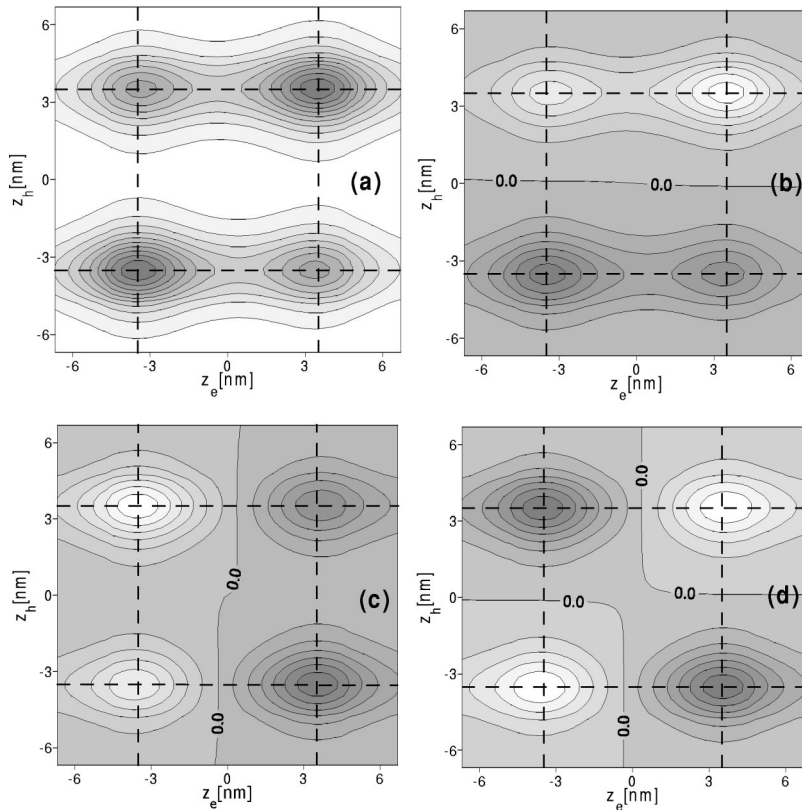


FIG. 6. Contours of s exciton wave functions for interdot-center distance $a=7$ nm. The symbols have the same meaning as in Fig. 5.

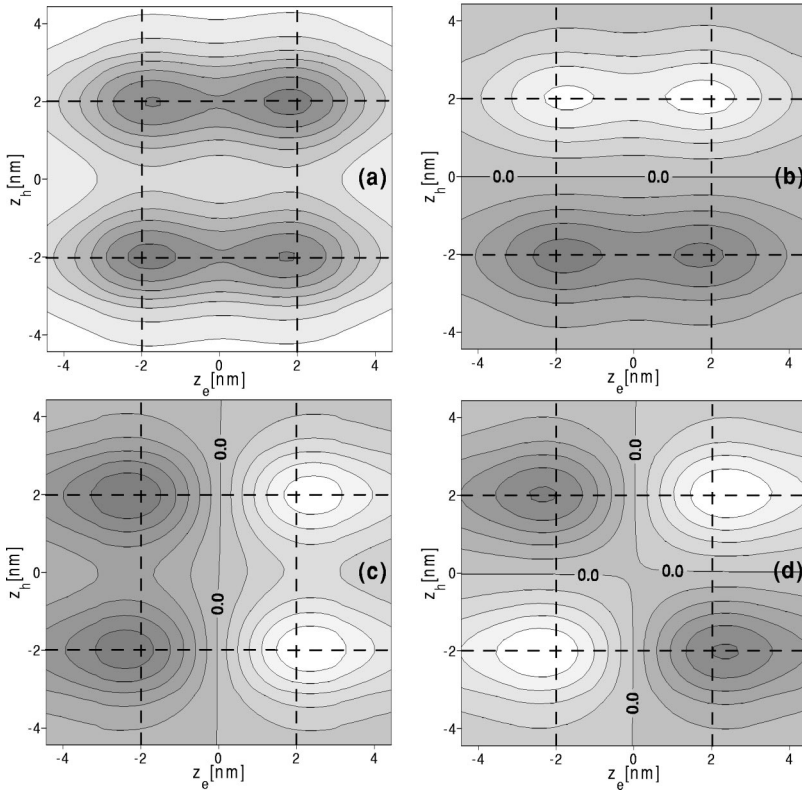


FIG. 7. Contours of s exciton wave functions for interdot-center distance $a=4$ nm. The symbols have the same meaning as in Fig. 5.

degenerate ground state possess extrema on the straight line $z_e = z_h$ and those for the degenerate excited states possess extrema on the straight line $z_e = -z_h$. This means that the twofold degenerate ground state corresponds to the electron-hole pair confined in the same quantum dot, whereas in the twofold degenerate excited state, the electron is confined in one QD and the hole is confined in the other. Therefore, in the limit of large interdot distances, the two pairs of degenerate states correspond to essentially different physical situations, i.e., the bound exciton and the dissociated exciton. The ground-state wave functions inside a single QD show the inversion symmetry with respect to the dot center [Figs. 5(a) and 5(b)]. The excited-state wave functions are slightly spread out in the direction of the other QD, in which the oppositely charged particle is localized [Figs. 5(c) and 5(d)]. We note that for large interdot distances the exciton wave functions do not show any trace of the symmetry with respect to the one-particle parity. Obviously, these wave functions are symmetric with respect to the simultaneous change of sign of both the z_e and z_h coordinates.

If the distance between the dots decreases, the energy of the excited state slightly lowers (cf. Fig. 4), which results from the increasing attraction between the electron and hole localized in different dots. This effect is not observed in the ground state, in which both the charge carriers are confined in the same QD. Therefore, in the case of large interdot distances, the only effective coupling is the long-range Coulomb coupling between the charge carriers localized in the different QD's. Figure 4 shows that for the barrier thickness $t \lesssim 8$ nm the higher-energy branches begin to grow and the degeneracy is lifted. In Fig. 6, we have plotted the exciton wave function for the four lowest-energy states in the case of

intermediate distance between the dots ($a=7$ nm). The results of Fig. 6 show that the correlation in the relative electron-hole motion is weaker than in the case of large interdot distances. In the two lowest-energy states [Figs. 6(a) and 6(b)], both the particles still prefer to occupy the same QD, but there appears a nonzero probability of occupation of different dots. In the third and fourth excited states [Figs. 6(c) and 6(d)], both the particles exhibit the tendency of avoiding each other, but with the nonvanishing probability of occupation of the same QD.

In Fig. 7, the shapes of the exciton wave functions are shown for a small interdot-center distance ($a=4$ nm). In this case, the wave functions begin to exhibit a definite parity with respect to the change of sign of the single z coordinate. The ground-state wave function is approximately even in both the z_e and z_h coordinates [Fig. 7(a)]. The first excited state [Fig. 7(b)] corresponds to the even-parity electron state and odd-parity hole state. On the contrary, in the second excited state [Fig. 7(c)], the electron possesses the odd parity and the hole possesses the even parity, whereas in the third excited state [Fig. 7(d)] both the particles possess the odd parity.

According to the results of Figs. 5, 6, and 7, the one-particle description of the parity symmetry is approximately true only for small interdot distances, i.e., in the limit of the strong interdot coupling. In a general case, the one-particle parity is not well-defined. Therefore, one has to be very careful when describing the symmetry of the exciton for the coupled QD's, especially when using one-particle methods, e.g., LDA approach,¹⁸ which cannot reproduce the total exciton parity. In particular, we can expect that—for some in-

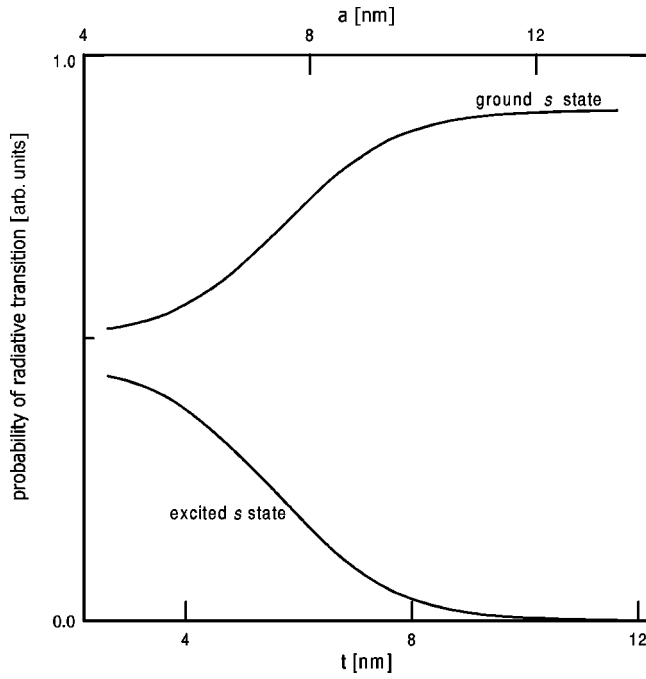


FIG. 8. Estimated probability of the radiative transitions from the even-parity ground and excited state of the exciton with $m=0$ confined in the coupled QD's as a function of barrier thickness t (distance between the dot centers a). The transition probability is expressed in arbitrary units.

terdot distances—the broken-parity self-consistent solutions possess a lower total energy.²⁸

The parity of the exciton state strongly affects the probability of radiative transitions, i.e., the electron-hole recombination. In Fig. 8, we have plotted the radiative-transition probability calculated according to formula (6) for the optically active exciton states with $m=0$ (s states) and even total parity. The probabilities of the radiative transitions from the ground s state take on fairly large values for all the distances between the QD's. In the ground state, the probability for the electron and the hole to be localized in different QD's increases with the decreasing interdot distance [cf. Figs. 5(a), 6(a), and 7(a)], which leads to the decreasing probability of the electron-hole recombination. The behavior of the probability of the recombination from the excited even-parity s state is just opposite. In this state, the charge carriers are spatially separated for large interdot distances [cf. Fig. 5(d)]. Therefore, the exciton wave function under integral (6) is equal to zero, which causes the probability of the radiative transition from the excited state to vanish. When the distance between the dots decreases, the charge carriers can be localized in the same QD and the excited-state recombination probability takes on nonzero and increasing values (Fig. 8). However, the probability of the radiative transition from the excited state always remains smaller than that from the ground state.

We have performed similar calculations for the exciton states with higher angular momentum quantum number m . The results (not presented here) show that the properties of

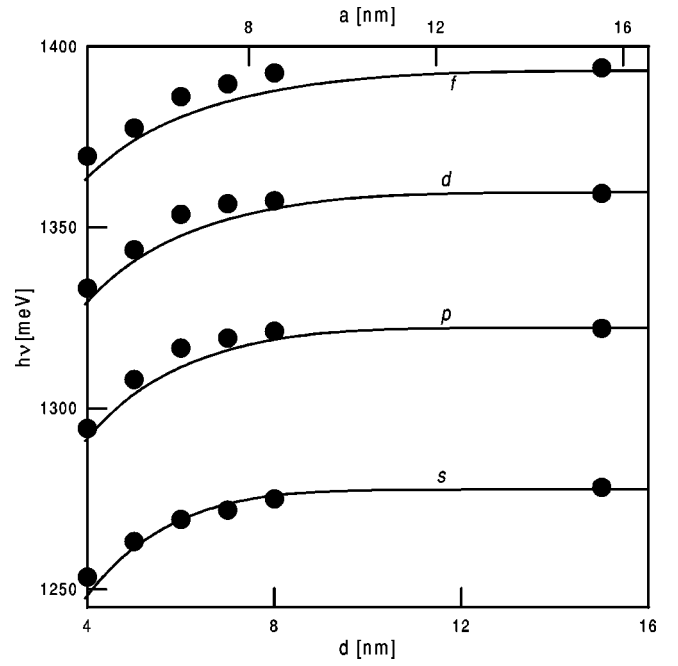


FIG. 9. Energy $h\nu$ of radiative transitions from the even-parity exciton states with one-particle angular-momentum quantum numbers $m=0$ (s), 1 (p), 2 (d), and 3 (f) as a function of spacer thickness d (a is the interdot-center distance, whereas $d=a-T_{WL}$). Solid curves show the results of the present calculations and full circles show results of the experimental data [Ref. 21].

the energy levels and relative recombination probabilities for the states of higher m are qualitatively the same those for the s states. This means that the vertical interdot coupling is only weakly affected by the in-plane motion.

As we have shown the radiative transitions are forbidden for the odd-parity initial states and are less probable for the excited even-parity states (cf. Fig. 8). This leads to the conclusion that the dominant contribution to the photoluminescence spectrum of the coupled dots originates from the lowest-energy even-parity exciton states for given m . The interdot coupling shifts the energies of these states towards the lower values (cf. Fig. 4).

Based on these results, we can now compare the predictions of the present model with the experiment.²¹ In Fig. 9, we have plotted the energies calculated for the allowed radiative transitions. The experimental data,⁴³ marked by the full circles, have been extracted from Ref. 21. Figure 9 shows that the calculated transition energies agree very well with the measured positions of the photoluminescence lines.²¹ The exciton recombination lines exhibit the pronounced redshift with the decreasing interdot distance. The following physical interpretation of this redshift can be given: the decrease of the interband transition energy means that the exciton binding energy increases with the decreasing interdot separation. This effect mainly results from the lowering of the one-particle energies (cf. Fig. 3), i.e., the stronger quantum confinement of the electron and the hole in the double quantum well with the growing effective range.

In the experimental spectra,²¹ taken for the QD's with

height $h \approx 2$ nm, no additional photoluminescence lines were observed. The appearance of additional photoluminescence lines was reported²¹ for the coupled QD's of the larger height ($h = 3$ nm). Unfortunately, the evolution of these additional lines with the varying interdot distance was not presented, probably because of a strong overlap of the luminescence maxima. The authors suggested²¹ that the s exciton line does not split and that the splitting becomes considerably larger for the highly excited exciton states. Based on the results of the present calculations, we argue that these suggestions are not correct. The calculated spacings between the energy levels of the even-parity s and p states are comparable (cf. Fig. 4) and the dependence of the relative recombination probability on the barrier thickness is similar for both the states. Therefore, if the higher-energy p state is observed, the higher-energy s state should also be observed.

Let us discuss a possibility of an experimental observation of the energy-level splitting for the exciton in the coupled QD's. As we have shown above (cf. Fig. 4), in the limit of large interdot distances, for given m the two pairs of energy levels are twofold degenerate. These levels are associated with the twofold parity-degenerate ground and excited states. In each pair, only one state (of even total parity) is optically active and can be detected experimentally. This feature is independent of the interdot distance. Therefore, a possible removal of the degeneracy of the two exciton states with the different total parity cannot be observed experimentally.

The higher-energy exciton states of even total parity can be observed under certain conditions. The even-parity states corresponding to the same angular momentum are *always*, i.e., for all interdot distances, energetically separated (cf. Fig. 4). In the limit of large interdot distances, the higher-energy exciton states cannot be detected, since the electron and the hole occupy different dots (cf. Fig. 5) and the transition probability vanishes (cf. Fig. 8). The recombination from the excited states can be observed only for small interdot distances (Fig. 8). If the additional photoluminescence lines connected with the higher-energy states of even parity appear in the spectrum, they are already blueshifted by at least 15 meV with respect to the lines corresponding to the lowest-energy states for given m (cf. Fig. 4). The new peaks (with increasing transition energies) can occur in the photoluminescence spectrum if the distance between QD's is sufficiently small.

According to our results, one of the new peaks with the lowest energy should correspond to the excited s state of the even total parity.

V. SUMMARY

In the present paper, we have introduced a theoretical model of a single QD based on the assumption of the Gaussian distribution of indium concentration. We have generalized this model in order to describe the coupling between the vertically stacked self-assembled QD's. The eigenvalue problem for the exciton in the coupled QD's has been solved with the use of the many-element variational basis, which partially takes into account the two-particle correlation effects. A good agreement has been obtained between the calculated and measured positions of photoluminescence peaks for different interdot distances. This agreement supports our hypothesis of the negligible influence of the inter-exciton interaction on the photoluminescence spectra in the self-assembled quantum dots. The present results show that the proposed Gaussian concentration distribution with the parameters fixed for the single QD is a universal function, which implicitly includes the most important effects in real QD's and properly describes the electronic properties of both the isolated single QD and coupled double QD's. For the coupled QD's we have studied the symmetry with respect to the parity of the exciton states. The present results show that—in a general case—the exciton wave functions do not possess a definite one-particle parity and only the total two-particle parity is conserved. For very small interdot distances the ground-state exciton wave functions exhibit the one-particle parity, but in an approximate manner only. We have also suggested that the recent assignment of the additional photoluminescence lines observed for the small interdot distances should be revised.

ACKNOWLEDGMENTS

This work has been partially supported by the Polish State Scientific Research Committee (KBN) under Grant No. 5 P03B 049 20. One of us (BS) gratefully acknowledges the support of the Foundation for Polish Science (FNP).

*Email address: bszafran@agh.edu.pl

¹For review articles, see T. Chakraborty, *Comments Condens. Matter Phys.* **16**, 35 (1992); M.A. Kastner, *Phys. Today* **46**(1), 24 (1993); M.A. Kastner, *Comments Condens. Matter Phys.* **17**, 349 (1996).

²P.A. Maksym and T. Chakraborty *Phys. Rev. Lett.* **65**, 108 (1990).

³S. Bednarek, B. Szafran, and J. Adamowski, *Phys. Rev. B* **59**, 13 036 (1999).

⁴B.T. Miller, W. Hansen, S. Manus, R.J. Luyken, A. Lorke, J.P. Kotthaus, S. Huant, G. Medeiros-Ribeiro, and P.M. Petroff, *Phys. Rev. B* **56**, 6764 (1997).

⁵A. Wójs, P. Hawrylak, S. Fafard, and L. Jacak, *Phys. Rev. B* **54**, 5604 (1996).

⁶R.J. Warburton, C.S. Dürr, K. Karrai, J.P. Kotthaus, G. Medeiros-Ribeiro, and P.M. Petroff, *Phys. Rev. Lett.* **79**, 5282 (1997).

⁷M. Grundmann, O. Stier, and D. Bimberg, *Phys. Rev. B* **52**, 11 969 (1995).

⁸B. Szafran, J. Adamowski, and S. Bednarek, *Phys. Rev. B* **61**, 1971 (2000).

⁹M. Bayer, O. Stern, P. Hawrylak, S. Fafard, and A. Forchel, *Nature (London)* **405**, 923 (2000).

¹⁰P. Hawrylak, G.A. Narvaez, M. Bayer, and A. Forchel, *Phys. Rev. Lett.* **85**, 389 (2000).

¹¹A. Wójs and P. Hawrylak, *Phys. Rev. B* **53**, 10 841 (1996).

¹²R.J. Warburton, B.T. Miller, C.S. Dürr, C. Bödefeld, K. Karrai, J.P. Kotthaus, G. Medeiros-Ribeiro, P.M. Petroff, and S. Huant, *Phys. Rev. B* **58**, 16 221 (1998).

- ¹³G. Park, O.B. Shchepochin, D.L. Huffaher, and D.G. Deppe, *Appl. Phys. Lett.* **73**, 3351 (2000).
- ¹⁴R.H. Blick, D. Pfannkuche, R.J. Haug, K. von Klitzing, and K. Eberl, *Phys. Rev. Lett.* **80**, 4032 (1998).
- ¹⁵D.G. Austing, T. Honda, K. Muraki, Y. Tokura, and S. Tarucha, *Physica B* **249**, 206 (1998).
- ¹⁶B. Kochman, T.B. Norris, B. Kochman, J. Singh, and P. Bhattacharya, *Appl. Phys. Lett.* **76**, 2394 (2000).
- ¹⁷J.J. Palacios and P. Hawrylak, *Phys. Rev. B* **51**, 1769 (1995).
- ¹⁸C.Y. Fong, B.M. Klein, L.A. Hemstreet, L.H. Yang, and J.S. Nelson, *J. Phys.: Condens. Matter* **10**, 4335 (1998).
- ¹⁹Y. Tokura, D.G. Austing, and S. Tarucha, *J. Phys.: Condens. Matter* **11**, 6023 (1999).
- ²⁰B. Partoens and F.M. Peeters, *Phys. Rev. Lett.* **84**, 4433 (2000).
- ²¹S. Fafard, M. Spanner, J.P. McCaffrey, and Z.R. Wasilewski, *Appl. Phys. Lett.* **76**, 2268 (2000).
- ²²S. Raymond, X. Guo, J.L. Merz, and S. Fafard, *Phys. Rev. B* **59**, 7624 (1999).
- ²³M. Eto, *Jpn. J. Appl. Phys., Part 1* **36**, 3924 (1997).
- ²⁴U. Merkt, J. Huser, and M. Wagner, *Phys. Rev. B* **43**, 7320 (1991).
- ²⁵D. Pfannkuche, V. Gudmundsson, and P.A. Maksym, *Phys. Rev. B* **47**, 2244 (1993).
- ²⁶J.-L. Zhu, Z.-Q. Li, J.-Z. Yu, K. Ohno, and Y. Kawazoe, *Phys. Rev. B* **55**, 15 819 (1997).
- ²⁷R.M.G. Garcia-Castelan, W.S. Choe, and Y.C. Lee, *Phys. Rev. B* **57**, 9792 (1998).
- ²⁸S.M. Reimann, M. Koskinen, M. Manninen, and B.R. Mottelson, *Phys. Rev. Lett.* **83**, 3270 (1999).
- ²⁹A.J. Williamson, L.W. Wang, and A. Zunger, *Phys. Rev. B* **62**, 12 963 (2000).
- ³⁰A. Franceschetti, H. Fu, L.W. Wang, and A. Zunger, *Phys. Rev. B* **60**, 1819 (1999).
- ³¹L. Quiroga and N.F. Johnson, *Phys. Rev. Lett.* **83**, 2270 (1999).
- ³²P.D. Sivers, S. Malik, G. McPherson, D. Childs, C. Roberts, R. Murray, B.A. Joyce, and H. Davock, *Phys. Rev. B* **58**, R10 127 (1998).
- ³³R. Colombelli, V. Piazza, A. Badolato, M. Lazzarino, F. Beltram, W. Schoenfeld, and P. Petroff, *Appl. Phys. Lett.* **76**, 1146 (2000).
- ³⁴S.B. Nam, D.C. Reynolds, C.W. Litton, R.J. Almassy, T.C. Collins, and C.M. Wolfe, *Phys. Rev. B* **13**, 761 (1976).
- ³⁵M. Cardona, *Phys. Rev.* **154**, 696 (1967); *Phys. Rev. B* **13**, 761 (1976).
- ³⁶J. Adamowski, M. Sobkowicz, B. Szafran, and S. Bednarek, *Phys. Rev. B* **62**, 4234 (2000).
- ³⁷C.W. Litton, R.B. Dennis, and S.D. Smith, *J. Phys. C* **2**, 2146 (1969).
- ³⁸A.L. Mears and R.A. Stradling, *J. Phys. C* **4**, L22 (1971).
- ³⁹F. Matossi and F. Stern, *Phys. Rev.* **111**, 472 (1958).
- ⁴⁰A.K. Walton and W.K. Mishra, *J. Phys. C* **1**, 533 (1968).
- ⁴¹D.J. BenDaniel and C.B. Duke, *Phys. Rev.* **152**, 683 (1966).
- ⁴²A. Wójs and P. Hawrylak, *Phys. Rev. B* **51**, 10 880 (1995).
- ⁴³The experimental points have been taken from Fig. 2 in Ref. 21 as the positions of the photoluminescence peaks.